



Unicentric Castleman disease: multidetector computed tomography classification with surgical and pathologic correlation

Xiaoli Sun^{1#}, Ye Du^{2#}, Ying Zhang³, Rengui Wang¹, Dailun Hou⁴

¹Department of Radiology, Beijing Shijitan Hospital, Peking University Ninth School of Clinical Medicine, Capital Medical University, Beijing, China; ²Department of Nephrology, Beijing Shijitan Hospital, Peking University Ninth School of Clinical Medicine, Capital Medical University, Beijing, China; ³Department of Pathology, Beijing Shijitan Hospital, Peking University Ninth School of Clinical Medicine, Capital Medical University, Beijing, China; ⁴Department of Radiology, Beijing Chest Hospital, Capital Medical University, Beijing, China

[#]These authors contributed equally to this work.

Correspondence to: Rengui Wang, Department of Radiology, Beijing Shijitan Hospital, Peking University Ninth School of Clinical Medicine, Capital Medical University, Yangfangdian Tieyi Road No.10, Haidian District, Beijing 100038, China. Email: 490150302@qq.com. Dailun Hou, Department of Radiology, Beijing Chest Hospital, Capital Medical University, Beiguan Street No. 9, Tongzhou District, Beijing 101149, China. Email: houdailun@163.com.

Background: This study aimed to correlate multidetector computed tomography (MDCT) classification of unicentric Castleman disease with the surgical and pathologic features.

Methods: The imaging manifestations of 63 cases of unicentric Castleman disease confirmed by pathology were retrospectively analyzed. Every patient underwent an MDCT examination. Classification based on imaging manifestations, surgical, histopathological, and imaging features were simultaneously reviewed and analyzed by two radiologists, with any disagreements resolved by consensus.

Results: Sixty-three patients with unicentric Castleman disease were divided into I-IV types by imaging manifestations: type I, single mass with smooth margin (n=5); type II, single mass with irregular or lobulated margin (n=33); type III, single invasive mass with blurred margin (n=20); and type IV, multiple fused masses (n=5). Thirty-eight cases of type I and type II were diagnosed as hyaline-vascular type by pathology after complete surgical resection; 20 cases were type III, in which eight cases were partially resected, 17 cases were pathologically diagnosed as hyaline-vascular type, and the remaining three cases were a mixed type. In five cases of type IV that could not be completely resected, four cases were hyaline-vascular type, and one case was plasma cell type.

Conclusions: MDCT is an excellent tool for the detection and diagnosis of unicentric Castleman disease. Classification by MDCT features is a reliable method for evaluating tumor infiltration and growth mode, which helps surgical optimization.

Keywords: Unicentric Castleman disease (UCD); classification; multidetector computed tomography

Submitted Sep 04, 2020. Accepted for publication Mar 12, 2021.

doi: 10.21037/qims-20-1033

View this article at: <http://dx.doi.org/10.21037/qims-20-1033>

Introduction

Castleman's disease (CD) is a rare benign lymphoid proliferative lesion, which is clinically divided into unicentric CD (UCD) and multicentric CD (MCD) (1,2). UCD refers to solitary or multiple lesions in adjacent organs

in a range of lesions that are limited to the same lymphoid region. MCD refers to multiple lesions involving more than two non-adjacent lymphoid regions or accompanied by other sites or organs. Pathologically, the CD is divided into hyaline-vascular type, plasma cell type, and mixed type

(2-4). The main pathological feature of UCD is the hyaline-vascular type, and the prognosis of early surgical resection is superior. The plasma cell type is the main type of MCD, which is treated with combined chemotherapy, and the prognosis is poor (4-7).

To the best of our knowledge, the CD is currently based on clinical and pathological findings classification. Multidetector computed tomography (MDCT) classification of the disease has not been reported in the literature. In this study, we correlated MDCT classifications of UCD with the surgical and pathological features. We explored MDCT classifications to evaluate tumor infiltration and growth model to improve the understanding of the disease and provide an imaging basis for surgical optimization.

Methods

Study population

The local ethics committee approved this study, and informed consent was not required since the study was conducted as a retrospective review. Between March 2007 and September 2018, 63 consecutive patients (30 men and 33 women) with UCD were retrospectively reviewed. Age at diagnosis ranged from 12 to 71 years (with a mean age of 34.1 years). All patients were diagnosed with UCD based on the clinical features and the results of postoperative pathology. All patients underwent MDCT, surgery, and histopathological examination and were followed up from 2 months to 5 years, both clinically and CT.

Among the 63 included patients, 22 cases (34.9%) were asymptomatic and found incidentally by physical examination, 16 cases (25.4%) were identified with simple compressive symptoms, including eight cases (12.7%) with intermittent chest tightness and cough, six cases (9.5%) were found with abdominal discomfort or dull pain accompanied by nausea and vomiting, and 25 cases (39.7%) were identified with an oral ulcer or/and skin erosion (paraneoplastic pemphigus, PNP).

CT data acquisition

All MDCT examinations were performed with either a 512-slice CT (Revolution, GE Healthcare, USA), a Brilliance 256-slice CT (Philips Healthcare, the Netherlands), or a 16-slice CT scanner (Somatom Sensation Cardiac 16, Siemens Medical Solutions; Forchheim; Germany). The patients were trained in breathing depth

and frequency before scanning. They were placed in the supine position and examined while they held their breath at the end of a deep inhalation. All patients were examined by thoracic or abdominal non-enhanced spiral MDCT scan. Fifty-five patients also underwent contrast-enhanced MDCT scanning simultaneously. Conventional thoracic or abdominal MDCT examinations were performed using multi-phase scan protocols, and the reconstructed images were transferred to picture archiving and communication system (PACS). Precontrast, arterial phase (30–40 s), and portal vein phase (70–90 s) were obtained. 80 mL of nonionic contrast material (Iopamidol, 300 mgI/mL; Bracco, Shanghai, China) was injected intravenously at a flow rate of 2.5–3.0 mL/s.

Scanning parameters on the MDCT scanner were set as follows: voltage, 120 kV; tube current, 150 mAs; collimation, 1 mm; pitch, 1; reconstruction interval, 0.5 mm; acquisition matrix, 512×512.

Image analysis

Unenhanced and contrast-enhanced spiral MDCT images of all patients were obtained. Original transverse and post-processed images were reviewed for each patient. Volume rendering (VR), maximum intensity projection (MIP), and multiple planar reconstruction (MPR) images were acquired. Features of the lesion, including size, shape, margin, attenuation, enhancement, and adjacent structures, were identified. Imaging manifestations and classification were reviewed and analyzed independently by two radiologists with 18- and 25-year experience in thoracic imaging. Any disagreements in the conclusions were resolved by consensus. The two radiologists were blinded to the pathological information.

Surgical and histopathological findings

The original CT transverse images and the reconstructed images of all patients were compared to the intra-operative situation, as observed during surgical resection and as characterized by the histopathological findings.

The hyaline-vascular type is characterized by hyaline vascular lymph follicles with expanded mantle zones containing small lymphocytes forming concentric rings (“onion skin” appearance) and an interfollicular capillary proliferation with perivascular hyalinization. The plasma cell type is characterized by variable germinal center hyperplasia and mantle zone expansion, often with relatively



Figure 1 Female, 59 years old. Abdominal enhanced CT images showed a round mass (arrow) in the peritoneal mesentery with smooth edges, clear fat spaces around it, and slight pressure on the adjacent small intestine. The boundary between the mass and the surrounding tissues was clear, and the mass was completely resected. The pathological classification was a hyaline-vascular type, and the image classification was the type I.

preserved lymph node architecture and a large number of plasma cell proliferation and no obvious vascular changes in the lymphoid follicles. The mixed type is a combination of both types.

Results

MDCT features and classification

Among the 63 included patients, 28 (44.4%) had abdominal and pelvic lesions, 25 (39.7%) had chest lesions, nine (14.3%) had neck lesions, and one (3.2%) had left axilla lesions. The lesions were round or oval in 23 cases (36.5%), lobulated or irregular in 32 cases (50.8%), and striped in eight cases (12.7%). The maximum diameter of the mass was 2–15 cm, with an average of 6.5 cm. Five cases (7.9%) had clear and smooth margins, 33 cases (52.4%) had clear but irregular or slight lobulation and 25 cases (39.7%) had blurred and irregular margins. Fifty-eight cases (92.1%) were single, and five cases (7.9%) were multiple.

Fifty-five underwent non-enhanced, and contrast-enhanced CT scans simultaneously. Non-enhanced CT showed uniform density in 52 cases (82.5%) and non-uniform density in 11 cases (17.5%). Calcification was

observed in 25 cases (39.7%), with central distribution in 21 cases and peripheral circular or arc calcification in four cases. Among the 55 patients who underwent contrast-enhanced CT, 24 cases (43.6%) showed homogeneous enhancement, and 31 cases (56.4%) showed inhomogeneous enhancement. Fifty-four cases showed significant enhancement in the arterial phase and continuous enhancement in the portal phase, and only one case, which was plasma cell type pathologically, showed mild inhomogeneous enhancement.

The MDCT characteristics of the mass were closely related to the histopathology of the lesion. Histopathologically, many scattered lymphatic follicles were seen in a hyaline-vascular type; the follicles were infiltrative and interstitial with abundant microvascular hyperplasia hyaline degeneration. Proliferative microvascular wall thickening and lumen stenosis, there were obvious hyaline degeneration, sclerosis, fibrosis, calcification, and other degenerative changes. It was distributed segmentally along the microvessels, and some calcification foci fused into larger calcium spots, which can explain the central distribution of calcification and the branching or speckle morphology of calcification in the imaging findings. The tumor enhancement mechanism was closely related to the abundant microvessel hyperplasia between the lymphatic follicles and the more peripheral blood supplying and nourishing arteries in the lesion. Uniform lesion density in non-enhanced CT scans may be related to the abundant blood supply and the non-necrotic nature of lymphoid follicular tissue itself.

According to MDCT manifestations, the 63 patients with UCD were divided into I-IV types: type I, five cases with single mass with smooth margin (n=5) (*Figure 1*); type II, 33 cases with single mass with irregular or lobulated margin (n=33) (*Figure 2*); type III, 20 cases with single invasive mass with blurred margin (n=20) (*Figure 3*); and type IV, five cases with multiple fused masses (n=5) (*Figure 4*).

Surgical and histopathological features

In 38 of the 63 patients, the lesion was completely resected without obvious adhesion or infiltration. In 20 patients, the degree of adhesion and infiltration between the lesion and surrounding tissues was different, of which 12 cases were completely resected, and eight cases were only partially resected. There was severe adhesion and infiltration between the lesion and surrounding tissues in five patients, which could not be resected.

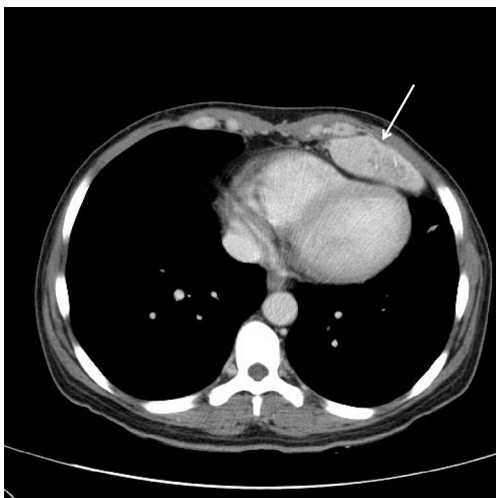


Figure 2 Female, 43 years old. Chest enhanced CT images showed a lobular mass (arrow) in the heart's anterior mediastinum with a smooth margin and clear fat space. The boundary between the mass and the surrounding tissues was clear, and the mass was completely resected. The pathological classification was a hyaline-vascular type, and the image classification was type II.

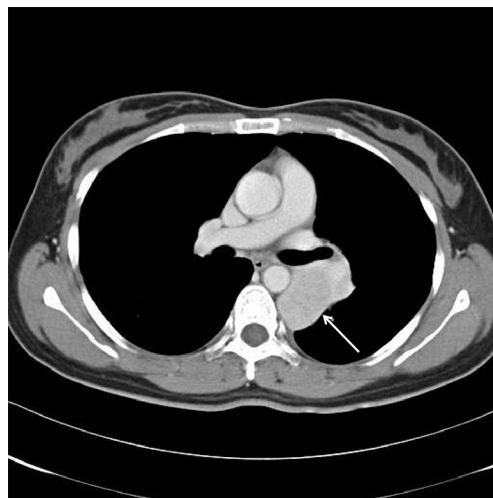


Figure 4 Female, 30 years old. Chest enhanced CT images showed irregular fusion masses (arrows) in the left posterolateral hilum, which were not clearly demarcated from the adjacent left pulmonary interlobar artery and its proximal branches, and the fat spaces around the masses disappeared. The mass could not be separated from the surrounding tissue structure during surgery. The pathological classification was a hyaline-vascular type, and the image classification was type IV.

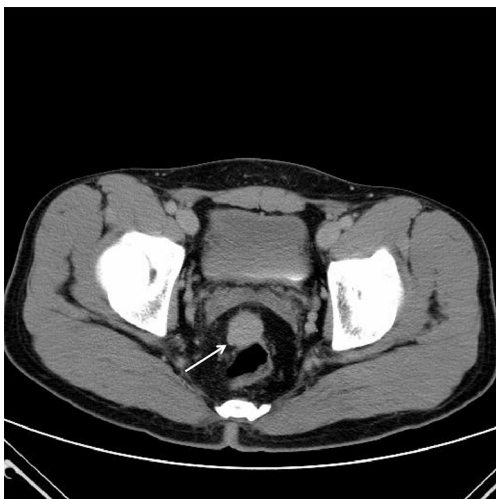


Figure 3 Male, 28 years old. Pelvic enhanced CT images showed a round mass (arrow) between the rectum and the seminal vesicle gland, with blurred margins and unclear demarcation between the mass and the adjacent rectal serosa. It was difficult to separate the mass from the adjacent rectum during surgery. The pathological classification was a hyaline-vascular type, and the image classification was type III.

Pathologically, 59 patients (93.7%) were hyaline-vascular type, one patient (1.6%) was plasma cell type, and three patients (4.7%) were the mixed type. Hyaline-vascular type is characterized by the accumulation of large lymphoid follicles in the proliferating lymphoid tissue, the abnormal germinal center in the lymphoid follicles, the follicular dendrites with the vesicular nucleus in the vitreous center, and an interfollicular capillary proliferation with perivascular hyalinization (*Figure 5*). Immunohistochemical staining for Cluster of Differentiation 21 (CD21) and Cluster of Differentiation 35 (CD35) showed a strong positive response to follicular dendritic cells.

The plasma cell type is characterized by abundant mature plasma cell infiltration between the follicles and no obvious vascular changes in the lymphoid follicles (*Figure 6*). Immunohistochemical staining of Cluster of Differentiation 38 (CD38) and Cluster of Differentiation 138 (CD138) showed that the plasma cells were strongly positive. The mixed type is characterized by both hyaline-vascular and plasma cell types (*Figure 7*).

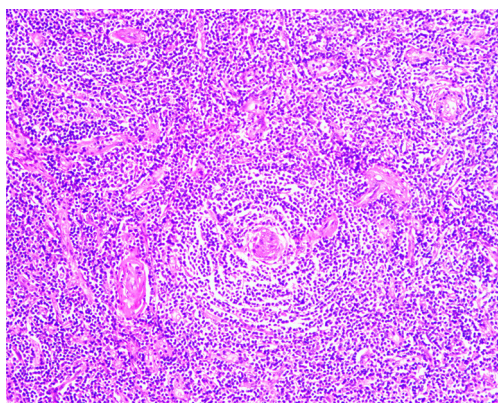


Figure 5 Hyaline-vascular type unicentric Castleman disease. Hematoxylin-eosin staining (10×10) staining showed significant vascular proliferation in the lymphoid follicles, and the lymphocytes arranged concentrically around the follicles formed an “onion skin” appearance.

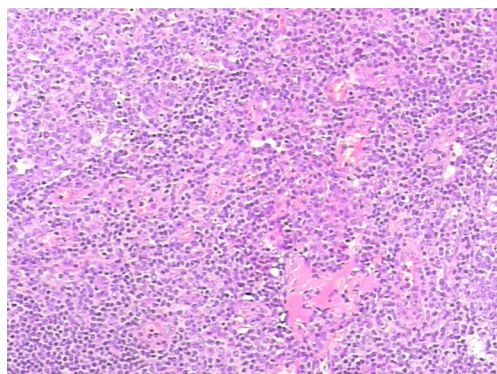


Figure 6 Plasma cell type unicentric Castleman disease. Hematoxylin-eosin staining (10×10) showed enlargement of the follicular space and mature plasma cells’ infiltration in the follicles.

MDCT classification and surgical and pathological analysis

There were 38 (60.3%) cases of type I and type II. The lesions’ boundaries were clear, the surgical resections were complete, and all cases were the hyaline-vascular pathological type. There were 20 (31.7%) cases of type III. The lesions had different degrees of adhesion and infiltration with surrounding tissues, the surgical separation was difficult, and there was more bleeding. Among them, eight cases could only be partially resected, 17 cases were the hyaline-vascular pathological type, and three were mixed types. Five (7.9%) cases were type IV. Intraoperatively, the lesions and the surrounding organs had different adhesion

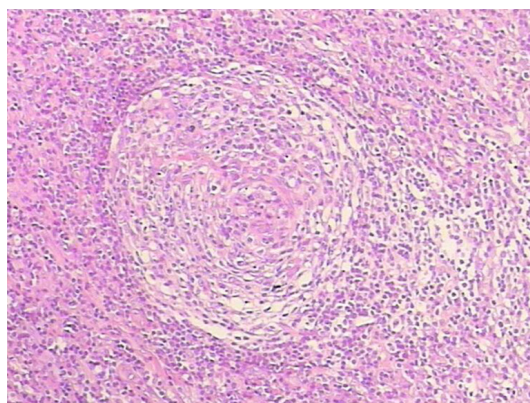


Figure 7 Mixed type unicentric Castleman disease. Hematoxylin-eosin staining (10×10) staining showed that the histological characteristics were both hyaline-vascular and plasma cell types.

degrees, which could not be completely removed. Four cases were hyaline-vascular type, and the remaining case was plasma cell type (*Table 1*).

Discussion

The imaging methods of UCD mainly include X-ray, angiography, ultrasound, computed tomography (CT), magnetic resonance imaging (MRI) and positron emission tomography (PET) (8). The CT performance of UCD has been reported in numerous studies, especially contrast-enhanced CT images (6,9,10). Through image analysis of this patient group combined with the existing literature, we believe that the following CT features help diagnose and identify: (I) isolated irregular soft tissue masses distributed along the perivascular lymphatic chain. In our study, 58 cases of single mass and five cases of multiple masses were all along with the lymph chain distribution; (II) after administration of intravenous contrast material; the lesion tends to demonstrate dramatic enhancement during the arterial phase, which persists but decreases during the venous phase; this intense enhancement will help narrow the differential diagnosis. In our study, among the 55 patients with contrast enhancement, 54 cases showed significant enhancement in the arterial phase and continuous enhancement in the portal phase; (III) non-uniform density of masses is unusual but may be observed in some cases. In our study, 11 out of the 63 included cases showed non-uniform density; and (IV) internal calcifications, which are characteristically coarse or demonstrate a distinctive

Table 1 MDCT classification and surgical and pathological features of 63 patients with unicentric Castleman Disease

Item	Cases	Proportion (%)
Gender		
Male	30	47.6
Female	33	52.4
Male: Female	1.00:1.10	
Age, years		
Range	12–71	
Median age	34.1	
MDCT subtype		
Type I	5	7.9
Type II	33	52.4
Type III	20	31.7
Type IV	5	7.9
Surgery		
Completely resected	50	79.4
Partially resected	8	12.7
Cannot be resected	5	7.9
Pathological subtype		
Hyaline-vascular type	59	93.7
Plasma cell type	1	1.6
Mixed type	3	4.7

branching pattern, can be seen in some lesions. In our study, 21 cases showed central distribution in the masses.

CD was first described in 1956 by Benjamin Castleman (11). He reported 13 cases of mediastinal lymphadenopathy with intra-mediastinographic imaging resembling Hassall corpuscles in the thymus and pathologically characterized by hypervascular lymph nodes with hyalinization of vessels. Some researchers have classified the hyaline-vascular, plasma cell, and mixed types according to the degree of capillary proliferation in or between lymphoid follicles and the infiltration of lymphocytes and plasma cells. Systemic symptoms were closely related to plasma cell type CD (12,13). Keller *et al.* (14) reported in 1991 that 91% of CD were the hyaline-vascular type with good prognosis and clinically benign features; plasma cell type only accounted for 9% and was clinically malignant diffuse with a poor prognosis. In our study, among the 63 patients with UCD,

59 patients (93.7%) with hyaline-vascular type were basically consistent with the literature reports.

The characteristic CT features of UCD are closely related to its pathological type. The above characteristic enhancements are pathologically hyaline-vascular or mixed type, which is related to its prominent feeding vessels close to a nodal mass and lymphatic tissue characteristics. Scattered spots in the tumor, cystic, or fissure-like non-necrotic hypoattenuation are mostly caused by intratumoral fibrous tissue hyperplasia, hyaline vascular changes, and gelatinous degeneration (15). The plasma cell type typically demonstrates less avid enhancement following contrast material administration, and calcification is uncommon (16,17). In this study, UCD was divided into four types according to the MDCT features. Types I and II surgical resections were complete, while the complete resection of types III and IV were difficult.

However, this study has three limitations that should be noted. Firstly, since this was a retrospective study, some patients with UCD were not included in the data analysis. Secondly, the number of patients with UCD was limited. Thirdly, we did not detect virological status (human immunodeficiency virus, Human herpesvirus) or inflammatory response in this study.

In conclusion, UCD is a rare disease characterized by benign lymphoid hyperplasia. MDCT is an excellent tool for the detection and diagnosis of UCD. Classification by imaging features is a reliable method for evaluating tumor infiltration and growth mode, which helps surgical optimization and prognosis prediction.

Acknowledgments

Funding: National Natural Science Foundation of China supported this study (grant No. 61876216) and Beijing Hospitals Authority Clinical Medicine Development of Special Funding (XMLX202146).

Footnote

Conflicts of Interest: All authors have completed the ICMJE uniform disclosure form (available at <http://dx.doi.org/10.21037/qims-20-1033>). The authors have no conflicts of interest to declare.

Ethical Statement: The authors are accountable for all aspects of the work in ensuring that questions related to the accuracy or integrity of any part of the work are

appropriately investigated and resolved. The study was conducted in accordance with the Declaration of Helsinki (as revised in 2013). The local ethics committee approved this study, and informed consent was not required because the study was performed as a retrospective review.

Open Access Statement: This is an Open Access article distributed in accordance with the Creative Commons Attribution-NonCommercial-NoDerivs 4.0 International License (CC BY-NC-ND 4.0), which permits the non-commercial replication and distribution of the article with the strict proviso that no changes or edits are made and the original work is properly cited (including links to both the formal publication through the relevant DOI and the license). See: <https://creativecommons.org/licenses/by-nc-nd/4.0/>.

References

1. Cronin DM, Warnke RA. Castleman disease: an update on classification and the spectrum of associated lesions. *Adv Anat Pathol* 2009;16:236-46.
2. Cheng JL, Cui J, Wang Y, Xu ZZ, Liu F, Liang SB, Tian H. Unicentric Castleman disease presenting as a retroperitoneal peripancreatic mass: A report of two cases and review of literature. *World J Gastroenterol* 2018;24:3958-64.
3. Bonekamp D, Horton KM, Hruban RH, Fishman EK. Castleman disease: the great mimic. *Radiographics* 2011;31:1793-807.
4. Sun X, Liu C, Wang R, Zhu X, Gao L, Chen J. The value of MDCT in diagnosis of hyaline-vascular Castleman's disease. *Eur J Radiol* 2012;81:2436-9.
5. Zhao S, Wan Y, Huang Z, Song B, Yu J. Imaging and clinical features of Castleman Disease. *Cancer Imaging* 2019;19:53-61.
6. McAdams HP, Rosado-de-Christenson M, Fishback NF, Templeton PA. Castleman disease of the thorax: radiologic features with clinical and histopathologic correlation. *Radiology* 1998;209:221-8.
7. Mitsos S, Stamatopoulos A, Patrini D, George RS, Lawrence DR, Panagiotopoulos N. The role of surgical resection in Unicentric Castleman's disease: a systematic review. *Adv Respir Med* 2018;86:36-43.
8. Kligerman SJ, Auerbach A, Franks TJ, Galvin JR. Castleman Disease of the Thorax: Clinical, Radiologic, and Pathologic Correlation: From the Radiologic Pathology Archives. *Radiographics* 2016;36:1309-32.
9. Luo JM, Li S, Huang H, Cao J, Xu K, Bi YL, Feng RE, Huang C, Qin YZ, Xu ZJ, Xiao Y. Clinical spectrum of intrathoracic Castleman disease: a retrospective analysis of 48 cases in a single Chinese hospital. *BMC Pulm Med* 2015;15:34.
10. Kwon S, Lee KS, Ahn S, Song I, Kim TS. Thoracic Castleman disease: computed tomography and clinical findings. *J Comput Assist Tomogr* 2013;37:1-8.
11. Castleman B, Iverson L, Menendez P. Localized mediastinal lymphnode hyperplasia resembling thymoma. *Cancer* 1956;9:822-30.
12. Festen C, Flendrig JA, Schillings PH. Giant lymphomas. *Ned Tijdschr Geneesk* 1969;113:1918-9.
13. Herrada J, Cabanillas F, Rice L, Manning J, Pugh W. The clinical behavior of localized and multicentric Castleman disease. *Ann Intern Med* 1998;128:657-62.
14. Keller AR, Hochholzer L, Castleman B. Hyaline-vascular and plasma cell types of giant lymph node hyperplasia of the mediastinum and other locations. *Cancer* 1972;29:670-83.
15. Ko SF, Hsieh MJ, Ng SH, Lin JW, Wan YL, Lee TY, Chen WJ, Chen MC. Imaging spectrum of Castleman's disease. *AJR Am J Roentgenol* 2004;182:769-75.
16. Meador TL, McLarney JK. CT features of Castleman disease of the abdomen and pelvis. *AJR Am J Roentgenol* 2000;175:115-8.
17. Kim TJ, Han JK, Kim YH, Kim TK, Choi BI. Castleman disease of the abdomen: imaging spectrum and clinicopathologic correlations. *J Comput Assist Tomogr* 2001;25:207-14.

Cite this article as: Sun X, Du Y, Zhang Y, Wang R, Hou D. Unicentric Castleman disease: multidetector computed tomography classification with surgical and pathologic correlation. *Quant Imaging Med Surg* 2021;11(8):3562-3568. doi: 10.21037/qims-20-1033